The Fourth IEEE RAS/EMBS International Conference
on Biomedical Robotics and Biomechatronics
Roma, Italy. June 24-27, 2012

An integrated motor control loop of a human-like robotic arm: feedforward, feedback and cerebellum-based learning

C. Casellato, A. Pedrocchi, J.A. Garrido, N.R. Luque, G. Ferrigno, E. D'Angelo, E. Ros

Abstract— A new complex model of human motor control has been developed, combining brain internal models and neural network mechanisms. Based on nervous system structures and operating principles, a feedforward block, a feedback controller and a cerebellum-like learning module have been integrated and tested with an anthropometric robotic arm. A simulated sequence of 8-like tracking tasks showed the contributions of these main loops over time. Different external dynamics were introduced. The role of feedback corrections, intrinsically imprecise due to sensorimotor delays, decreases, while the output of cerebellum, which has been learning, increases; the movement becomes more accurate. Moreover, an experimental session on a subject performing the task repetitions using a haptic device was carried out, recording upper limb kinematics.

I. Introduction

THE biological motor system is a high performance control engine. Unlike artificial control systems, it exhibits much higher performance with great flexibility and versatility in spite of nonlinearities, uncertainties and large Degrees of Freedom (DoF) of animal bodies. Sensorimotor function is created from a highly distributed circuit that includes different neural centers, such as cerebral cortex, cerebellum, and spinal cord.

The movement kinematic planning to achieve a particular task is assigned to the premotor and somatosensory cortical areas; they generate the optimal trajectory and transform this external-space Cartesian coordinates into internal-space joint coordinates through inverse kinematics processing. It was shown that somatosensory cortex cells encode joint-centered kinematics; their activity is correlated with position, velocity and acceleration parameters [1].

Then, the motor commands, in order to achieve such desired kinematics, are defined. The brain must construct internal models of the plant, objects and environment only through learning by experience and memorize them in its neural networks in a usable format for motor control. The primary motor cortex (M1) is considered the site where basic inverse dynamic models are stored, thus behaving as a nonlinear feedforward controller able to compute torque values. Since possible joint miscalibrations, context changes, noise and other uncertainties, this structure is not capable of guaranteeing an accurate control on its own.

The cerebellum is able to fine-tune motor skills by processing incomplete or approximate commands issued by higher levels of motor system [2]. It is in charge of temporal and spatial movement coordination. Its structure, made up of microzones acting as functional units, fits well with the learning mechanisms. Patients suffering cerebellar dysfunctions (e.g. cerebellar ataxias) are almost unable to deal with disturbances as they can rely only on the imprecise and unstable feedback control to enhance the basic inverse model of motor cortex [3].

The action of a feedback controller in motor control is well accepted. The role of M1 in this loop is proved, neurophysiologically, by a dense projection from M1 to the spinal cord, often directly onto motor neurons, and by a number of correlations between M1 firing and end-effector kinematics [4]. Ito [5] showed that the feedback controller generates a command in motor cortex, which can tune the viscoelastic properties of musculoskeletal system (tension-length and tension-velocity relationships). Adaptive feedback controllers have been proposed [6], which means that the pre-programmed arm impedance changes in response to feedback information. For instance, it has been shown that impedance increases around the task constraints [7]. Feedback gains, which convert sensory state variables into motor signals, are optimized based on specific goals of a particular behavior, by following the 'minimum intervention principle' [8], [9]. Thus, the optimal feedback control consists of two main steps: state/error estimation and control laws.

No model of human-like motor control including this overall complexity has been built. In all biological systems, in which all the different parts have been evolved together towards global aims, the whole is more complex than the sum of its parts. Kawato [10] proposed the adaptive nonlinear feedforward controller, based on a feedback-error learning architecture; that is, error signals from linear feedback controller tune the feedforward inverse model parameters. Schweighofer and colleagues [11] showed how the cerebellum may increase the accuracy in target reaching movements by compensating for the interaction torques, thus by learning a portion of the inverse dynamics model that refines a previously stored basic inverse model in the motor cortex. Other models were proposed and tested on planar movements of a robotic arm, e.g. [12], [13].

Starting from functional/anatomical schemes and from these previous important steps, the present study integrates control models [14], learning models, neural network dynamics and behavioral observations, by using both modeling/computational and experimental approaches on multi-joint 3D movements.

978-1-4577-1200-5/12/$26.00 ©2012 IEEE

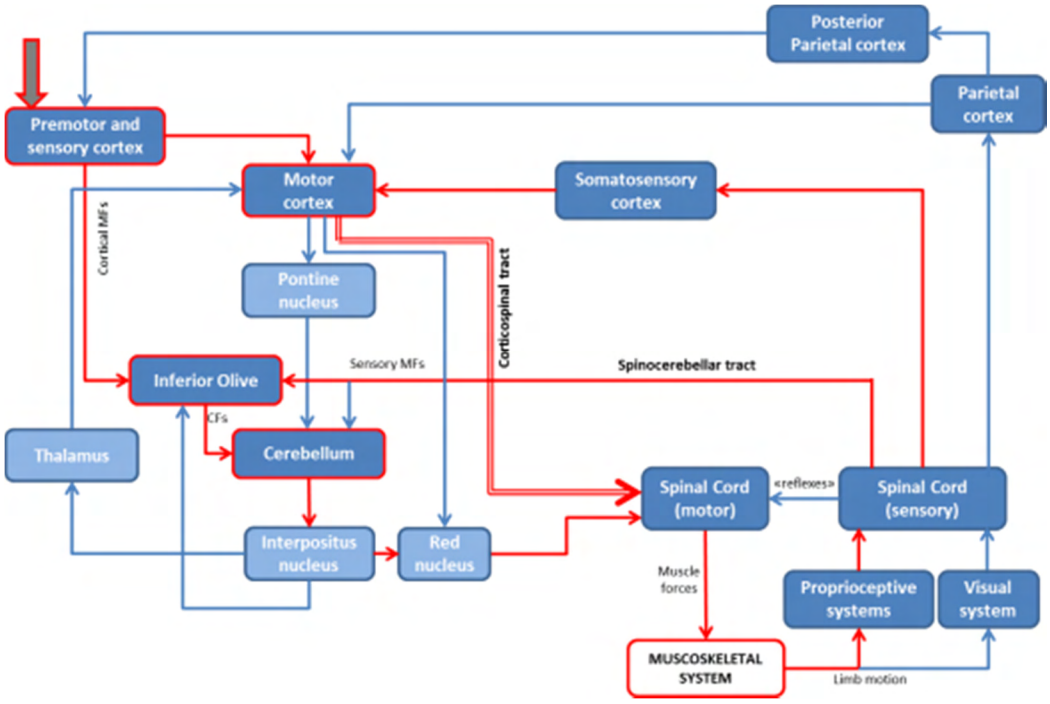

Figure 1. Model

The scheme includes the main neural structures and functional interconnections involved in motor control. In red the blocks and the connections implemented in our control model.

II. Modeling Approach

A. Control system

Fig.1 comes up with the main neural structures and mutual connections involved in motor control, highlighting the ones implemented in our model.

Premotor and sensory cortex blocks compute the kinematic planning. First, the desired trajectory is generated following a minimum-jerk criterion in external space, so facing the kinematic redundancy [15]. Then, closed-form inverse kinematics is carried out to compute displacement, velocity and acceleration for each of the three joints [16].

The nonlinear feedforward controller is placed into M1 block; it is made up of an inaccurate inverse dynamic model of the arm based on recursive Newton-Euler dynamic equations computing joint torques. These dynamic equations do not take into account friction torques, inertial interaction torques (i.e. inertia tensor matrix presents zero terms for the off-diagonal elements), and internal neural noise. The latter here consists of both sensorial noise on actual kinematics and signal-dependent noise on total torques, i.e. proportional to motor command amplitudes [17], [18]. Moreover, the inverse model does not include unexpected external force changes, embedding just the very well-known gravity action.

$$\boldsymbol{\tau}_{\mathbf{feedforward}} = \widetilde{\tau_{in}} + \tau_c + \tau_{gr} + \cancel{\tau_{friction}} + \cancel{\tau_{ext}}$$

The linear feedback controller, receiving somatosensory information from the periphery, is sited within M1. By means of exploiting muscular viscoelasticity, an additive torque value is produced depending on the ongoing error, as an online correction. Its performance is limited due to the system nonlinearities and the inevitable feedback sensorimotor delays. Because of muscle spindles do not carry a significant amount of acceleration information, only position and velocity are present in the feedback controller. Position and velocity errors (e_p, e_v) are weighted by gains (K_p and K_v: elasticity and viscosity features, respectively); this arm impedance is selected depending on the task requirements and keeping in mind that high feedback gains enhance robustness to external perturbations but, at the same time, increase noise (signal-dependent noise) and metabolic cost. It would imply non-compliant and non-stable movements [19], [20].

$$\boldsymbol{\tau}_{\mathbf{feedback}} = \cancel{K_p} \cdot e_p + \cancel{K_v} \cdot e_v$$

The plasticity mechanisms are implemented by the cerebellum and inferior olive blocks. The cerebellum learns to provide corrective torques towards reducing the kinematic errors in incoming trials; thus, it acts as a predictor.

This biological adaptation takes place on the parallel fiber to Purkinje cell synapses, driven by the activity from the Inferior Olive that here encodes a teaching signal (dependent on the accuracy of the movement execution compared to the desired movement trajectory).This system implements a look-up table which associates each parallel fiber state [27] with a Purkinje cell output. This association is iteratively modified during the learning process.

The adaptation mechanism is based on LTD/LTP (Long-Term Depression and Potentiation) processes validated in previous approaches [21] with a linear firing rate cerebellar model. This cerebellum-like model delivers add-on output corrective torque terms based on the received feedback error

along previously executed trials. The cerebellar module torque action is defined following the equation:

$$\boldsymbol{\tau_{cerebellum}} = (\mathrm{MF_{gain}} - \mathrm{PC_i(t)}) \cdot \mathrm{Gains_{out}}$$

Where $\mathrm{Gains_{out}}$ allow a rescaling based on the torque ranges, $\mathrm{MF_{gain}}$ represents the activity coming through mossy fibers (this input activity has been fixed to 1 in order to normalize the output activity in between 0 and 1) and $\mathrm{PC_i(t)}$ is the Purkinje cell firing rate associated to the currently active parallel fiber. This activity is iteratively modified following the equation:

$$\Delta \mathrm{PC_i(t)} = \begin{cases} \dfrac{\mathrm{LTP_{Max}}}{(\mathrm{e}+1)^{\alpha}} - \mathrm{LTD_{Max}} \cdot \mathrm{e}, if\ PF_i\ is\ active\ at\ time\ t \\ 0, otherwise \end{cases}$$

Where $\mathrm{LTP_{Max}}$ and $\mathrm{LTD_{Max}}$ are parameters which regulate the learning plasticity mechanism speed (both have been fixed to 0.2), e represents the error signal (a linear combination of joint position and velocity error, normalized between 0 and 1) and α regulates the LTP/LTD interaction (it has been set up to 1000 to reduce LTP action in presence of a significant error). Finally, $\mathrm{PC_i(t)}$ is configured to be always working in the range [0, 1].

The expected behavior of the whole system should be that the feedback controller progressively is driven out, since the cerebellum adjusts progressively internal models. Thus, the desired motions will be mainly predicted and only small correction forces will be required, so increasing the system's control compliance.

B. Plant

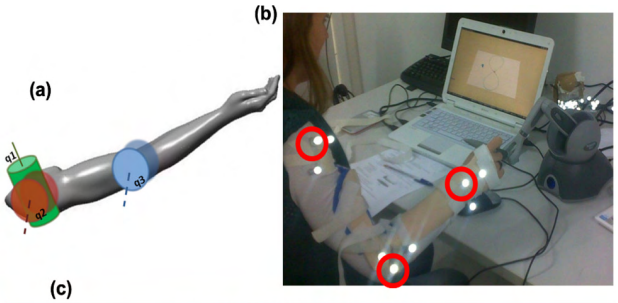

(c)

DENAVIT-HARTENBERG PARAMETERS						
Joint	α [rad]	a [m]	θ	d [m]	R/P	Offset
1	π/2	0	q1	0	R	0
2	0	0	q2	Arm length	R	0
3	0	0	q3	Forearm + hand length	R	0

Figure 2. Human-like robotic arm

(a) Robotic arm built for our model, with 3 DoF. Green (q1): shoulder abduction/adduction. Red (q2): shoulder lowering/elevation. Blue (q3): elbow extension/flexion.
(b) Experimental set-up: the 3-marker tools on the involved joints, the haptic device and the graphical interface with the required task.
(c) The conventional Denavit-Hartenberg parameters which define the kinematic features of the anthropometric robotic arm.

A robotic arm is built with 3 rotational DoFs: q1 represents shoulder abduction/adduction, q2 shoulder lowering/elevation, and q3 elbow extension/flexion, as reported in Fig.2-a. The kinematic parameters are defined according to Denavit-Hartenberg convention (Fig.2-c), setting the link lengths depending on subject's anthropometric measurements. The inertial parameters for each link, such as mass, CoM position, and inertia tensor are set depending on subject's anthropometric measures as well [22], [23], [24], [25].

C. Simulations

The control loop and the robot plant have been built up in Simulink (Mathworks®), using a Robotic Toolbox [26].

A simulation of an 8-like trajectory tracking task in 3D was carried out, where one trial lasted 4 s and 20 repetitions were performed. The unexpected external force perpendicular to end-effector was a step: from 0.6 N to 2.3 N at half of each trial duration. The time resolution was 2 ms.
The signal-dependent noise was a white noise with amplitude equals to 2% of the torque amplitude.
The feedback controller was characterized by K_p and K_v proportional to the external force modulus: $K_p = 3 \cdot |F_{ext}|$ [Nm/rad]; $K_v = 1 \cdot |F_{ext}|$ [Nm/(rad/s)]. The delay was 50 ms.
The cerebellum module was implemented by a linear firing rate model of the cerebellum which includes some of the traditional working hypothesis of the cerebellum, such as the generation of non-recurrent states at the granular layer [27], synaptic plasticity at the parallel fibers driven by the climbing fiber activity and synaptic integration at the Purkinje layer [28], [29].

For each task repetition, multiple variables were recorded. The different contributions on the total torque (τ_{tot}) were computed, as ratio of Root Mean Square (RMS) values:

- $\tau_{cerebellum}/\tau_{tot} = RMS(\tau_{cerebellum}) / [\ RMS(\tau_{cerebellum}) + RMS(\tau_{feedback}) + RMS(\tau_{feedforward})\ ]$
- $\tau_{feedback}/\tau_{tot} = RMS(\tau_{feedback}) / [\ RMS(\tau_{cerebellum}) + RMS(\tau_{feedback}) + RMS(\tau_{feedforward})\ ]$

The Cartesian error of the end-effector was evaluated by using two main parameters: RMS-Error and the correlation between the desired and the actual 3D trajectories.

D. Results

The main simulation results are reported in Fig.3. It is evident, from the joint angles (3-a), that the distance between the desired and the actual movements decreases over time. It is also supported by the Cartesian trajectories (3-c) and the performance indexes (3-d and 3-e).

Panel 3-b shows how the different controllers contribute to the whole motor commands over time; the feedback component is predominant in the very first trials, while the cerebellum is still learning.

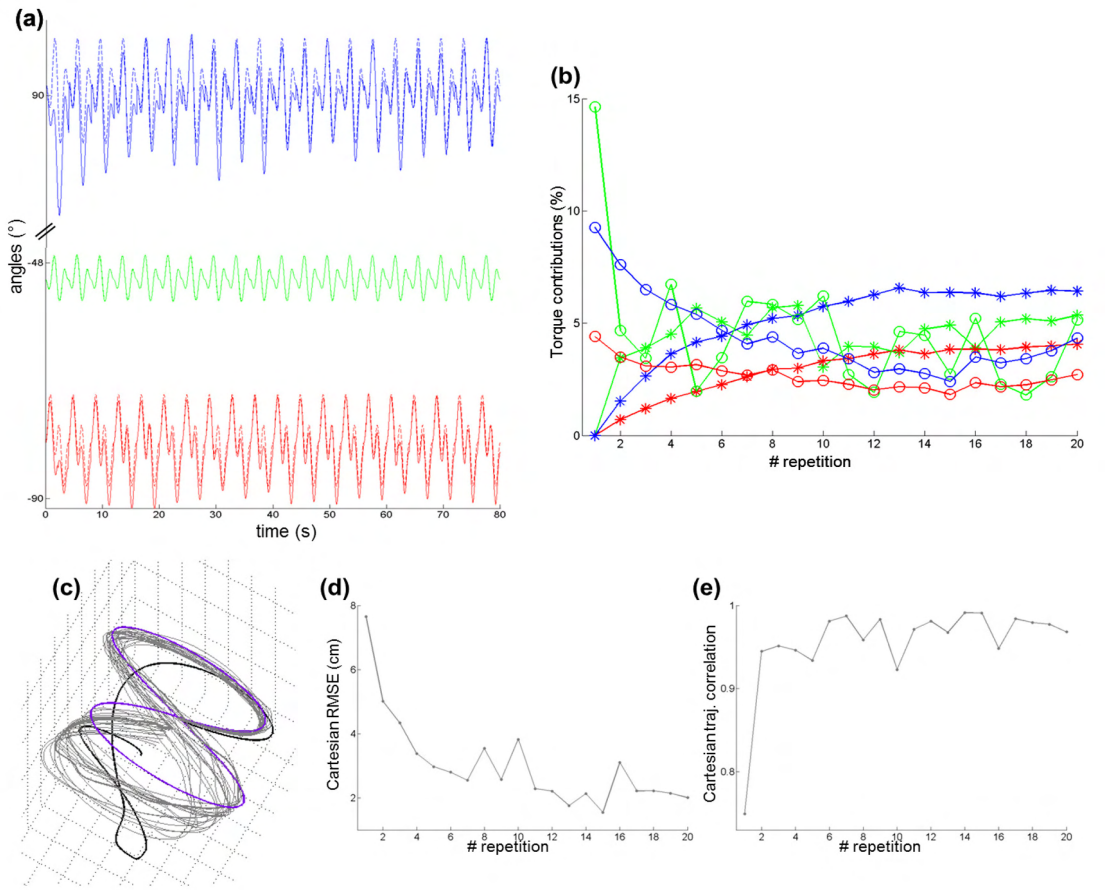

Figure 3. Simulation with external perturbation at half of each task repetition

(a) The 3 DoF angles (q1, q2, and q3, as in Fig.2-a), with time (80 s, i.e. 20 repetitions). Solid curves: the actual joint angle; dashed curves: the desired joint angle.
(b) The % contributions, with respect to the total generated torque, of cerebellum torque (star curves) and of feedback torque (circle curves). These values are reported for each joint and for each task repetition.
(c) The 3D Cartesian end-effector trajectories. In violet: the desired one. In black: the first repetition. In thick grey: the last repetition. In thin grey: the intermediate repetitions.
(d) The Root Mean Square Error between the 3D desired trajectory and the actual one, for each repetition.
(e) The correlation coefficient between the 3D desired trajectory and the actual one, for each repetition.

Latest repetitions show a cerebellum correction activity bigger than the feedback one for all joints, with quite stable trends. It is worthy to note that the q3 curves (green) are higher than the other joints even if the error is smaller (as it is shown by the green curves in panel 3-a) since this joint feedforward torque does not include the gravity component; q3 indeed moves on the horizontal plane.

III. Experimental Approach

A. Set-up

Preliminary experimental sessions on one healthy subject were carried out in order to qualitatively compare the simulator kinematic movement and a realistic one. The subject's upper limb segments were acquired by a motion capture system (VICRA, Polaris^{TM}), thus placing a 3-passive-markers tool on each joint (shoulder, elbow and wrist). A haptic device (PHANToM OMNI, SensAble^{TM}) was used to perform the task, developing in Visual C++ a task-specific visual interface and a control algorithm proving the subject with the external force changes. By displaying a countdown, the subject was aware of the required trial duration. Start and end points were marked through touchable spheres within the task environment. The set-up picture is reported in Fig.2-b.

In order to constrain the movement to the selected 3 DoFs, the subject worn a wrist plaster cast, so as the haptic device pen was like a forearm extension. The subject was instructed to avoid as much as possible the use of finger DoFs, the shoulder rotation and any translation.

After few familiarization trials, the subject was asked to perform 5 trials with a low constant external vertical force field (0.6 N) and 5 trials with a force field change from the half of each trial duration (from 0.6 N to 2.3 N).

B. Results

Fig.4 depicts the main representative results, concerning the 5 trials with external disturbance. In Fig.4-a, the experimental angles are laid on the ones which come from simulator planning (desired joint angles). It is evident that, whereas the shoulder DoFs (q1 and q2) fit quite well with the desired ones, the elbow flexion (q3) is significantly smaller in the experimental data than in the simulation approach. This could be because the subject used also other DoFs, such as fingers, to achieve the task.

Fig.4-b draws the cartesian end-effector trajectories, and in Fig.4-c and 4-d, performance indexes, analogous to the ones computed for simulation, are reported along the 5 repetitions. Both parameters show values that are similar to the ones achieved in simulation after the first trials. It could be explained by the fact that the subject performed some trials for familiarization before recordings, even if not enough training time to get a stable behavior. Next experiments will foresee more repetitions, so as to achieve a convergent trend of performance indexes.

IV. Discussion

The model presented here for motor control revealed itself neurophysiologically plausible and comparable with experimentally-based modeling. It successfully puts together different flexible controllers and predictors, including both control-based and neural-network blocks in a whole complex system.

The model behavior can be explored for other tasks (e.g. first tests on reaching task have been carried out) and for any dynamic environment. Multiple factors can be set; for instance, the inverse dynamic model inaccuracies, the task-dependent optimal feedback law and the time constant of cerebellar learning rules.

A lot of enhancing steps will be implemented within the model. The analogical model of the cerebellum can be replaced with a spiking network version similarly as presented in [13] and [21] (EDLUT: Event-Driven Look-Up Tables), which can naturally include more realistic plasticity mechanisms [30], starting from the most recent dualism between neurophysiology evidences and neural network modeling, e.g. [27]. Furthermore, the cerebro-cerebellar loop could be exploited within the model. In this direction, a first attempt was carried out through a recurrent architecture model, where the cerebellum output modified the motor cortex input, i.e. the kinematic planning, so solving the motor error problem [31].

Finally, the neurophysiology demonstrated that, after learning, the inferior olive response decreases significantly [12], thus suggesting that when the cerebellum learning has been completed, the learning consolidation occurs transferring this information directly to the motor cortex, i.e. making directly the feedforward generated motor commands more accurate.

In conclusion, this model is using a control scheme consistent with the motor-learning theory, in which the motor error is pre-computed and sent to the parallel fiber - Purkinje cell connection of the cerebellum, in order to generate LTD and LTP through a supervised learning rule. Thus, the model now provides the basis for testing more biologically plausible architectures and computational solutions, including vector coding in the motor cortex, implicit learning in the cerebellar granular layer, and various signal transformations in the different nuclei involved. In particular, the expansion of the cerebellum into a detailed neuronal network using the EDLUT simulator will allow to test the impact of biological circuit and cellular properties on the control capabilities of the cerebro-cerebellar loop.

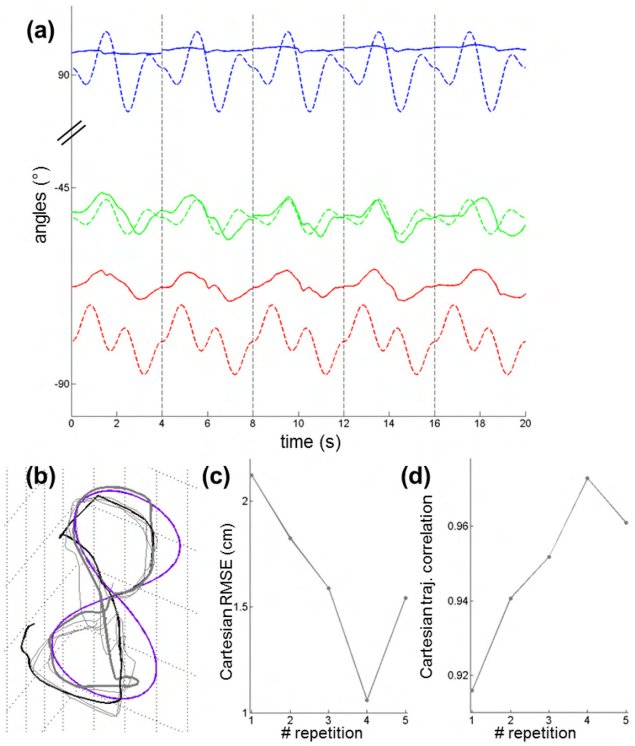

Figure 4. Experimental data

(a) The 3 DoF angles (q1, q2, and q3, as in Fig.2-a), with time (20 s, i.e. 5 repetitions). The vertical lines bound each repetition. Solid curves: experimental data; dashed curves: the desired joint angles from simulator planning.

(b) The 3D Cartesian end-effector trajectories. In violet: the desired one. In black: the first repetition. In thick grey: the last repetition. In thin grey: the intermediate repetitions.

(c) The Root Mean Square Error between the 3D desired trajectory and the actual one, for each repetition.

(d) The correlation coefficient between the 3D desired trajectory and the actual one, for each repetition.

ACKNOWLEDGMENT

This work has been supported by the EU grant REALNET (FP7-ICT-270434).

REFERENCES

[1] J. F. Kalaska, D. A. Cohen, M. Prud'homme, and M. L. Hyde, "Parietal area 5 neuronal activity encodes movement kinematics, not movement dynamics.," Exp Brain Res, vol. 80, pp. 351-364, 1990.

[2] M. Ito, "Cerebellar circuitry as a neuronal machine.," Prog Neurobiol, vol. 78, pp. 272-303, 2006.

[3] A.J Bastian, "Cerebellar limb ataxia: abnormal control of self-generated and external forces.," Ann N Y Acad Sci, vol. 978, pp. 16-27, 2002.

[4] E. Todorov, "Direct cortical control of muscle activation in voluntary arm movements: a model.," Nat Neurosci, vol. 3, pp. 391-398, 2000.

[5] M. Ito, "Control of mental activities by internal models in the cerebellum.," Nat Rev Neurosci, vol. 9, pp. 304-313, 2008.

[6] J. Nakanishi and S. Schaal, "Feedback error learning and nonlinear adaptive control.," Neural Netw, vol. 17, pp. 1453-1465, 2004.

[7] R. Osu, K. Morishige, H. Miyamoto, and M. Kawato, "Feedforward impedance control efficiently reduce motor variability.," Neurosci Res, vol. 65, pp. 6-10, 2009.

[8] S.H Scott, "Optimal feedback control and the neural basis of volitional motor control.," Nat Rev Neurosci, vol. 5, pp. 532-546, 2004.

[9] D. Mitrovic, S. Klanke, R. Osu, M. Kawato and S. Vijayakumar, "A computational model of limb impedance control based on principles of internal model uncertainty. " PLoS One, vol. 5, e13601, 2010.

[10] M. Kawato, K. Furukawa, and R. Suzuki, "A hierarchical neural-network model for control and learning of voluntary movement.," Biol Cybern, vol. 57, pp. 169-185, 1987.

[11] N. Schweighofer, M. A. Arbib, and M. Kawato, "Role of the cerebellum in reaching movements in humans. I. Distributed inverse dynamics control.," Eur J Neurosci, vol. 10, pp. 86-94, 1998.

[12] N. Schweighofer, J. Spoelstra, M. A. Arbib, and M. Kawato, "Role of the cerebellum in reaching movements in humans. II. A neural model of the intermediate cerebellum.," Eur J Neurosci, vol. 10, pp. 95-105, 1998.

[13] R.R Carrillo, E. Ros, C. Boucheny, and O.J. Coenen, "A real-time spiking cerebellum model for learning robot control.," Biosystems, vol. 94, pp. 18-27, 2008.

[14] J.J Craig, Introduction to robotics: mechanics and control., 2005.

[15] E. Todorov, "Optimality principles in sensorimotor control.," Nat Neurosci, vol. 7, pp. 907-915, 2004.

[16] D. Kostic, M. Bram de, and R. Hensen, "Modeling and identification for high-performance robot control: an RRR-robotic arm case study," IEEE Transactions on Control Systems Technology, vol. 12, pp. 904-919, 2004.

[17] C. M. Harris and D. M. Wolpert, "Signal-dependent noise determines motor planning.," Nature, vol. 394, pp. 780-784, 1998.

[18] K.E Jones, A.F Hamilton, and D.M Wolpert, "Sources of signal-dependent noise during isometric force production.," J Neurophysiol, vol. 88, pp. 1533-1544, 2002.

[19] E. Burdet, R. Osu, D. W. Franklin, T. E. Milner, and M. Kawato, "The central nervous system stabilizes unstable dynamics by learning optimal impedance.," Nature, vol. 414, pp. 446-449, 2001.

[20] J. Porrill and P.Dean, "Recurrent cerebellar loops simplify adaptive control of redundant and nonlinear motor systems.," Neural Comput, vol. 19, pp. 170-193, 2007.

[21] N.R. Luque, J.A. Garrido, R.R. Carrillo, O.J. Coenen, and E. Ros, "Cerebellarlike corrective model inference engine for manipulation tasks.," IEEE Trans Syst Man Cybern B Cybern, vol. 41, pp. 1299-1312, 2011.

[22] D.A. Winter, Biomechanics and Motor Control of Human Movement. John Wiley \& Sons, 1990.

[23] P. de Leva, "Adjustments to Zatsiorsky-Seluyanov's segment inertia parameters.," J Biomech, vol. 29, pp. 1223-1230, 1996.

[24] H.A. Abdullah, C. Tarry, R. Datta, G. S. Mittal, and M. Abderrahim, "Dynamic biomechanical model for assessing and monitoring robot-assisted upper-limb therapy.," J Rehabil Res Dev, vol. 44, pp. 43-62, 2007.

[25] A.H. Vette, T. Yoshida, T.A. Thrasher, K. Masani, and M.R. Popovic, "A complete, non-lumped, and verifiable set of upper body segment parameters for three-dimensional dynamic modeling.," Med Eng Phys, vol. 33, pp. 70-79, 2011.

[26] P. Corke, "Robotics Toolbox for Matlab," 2008.

[27] T.Yamazaki and S. Tanaka, "The cerebellum as a liquid state machine.," Neural Netw, vol. 20, pp. 290-297, 2007.

[28] D. Marr, "A theory of cerebellar cortex.," J Physiol, vol. 202, pp. 437-470, 1969.

[29] J.S. Albus, "A theory of cerebellar function," Math Biosci, vol. 10, pp. 25-61, 1971.

[30] E. D'Angelo, "Neural circuits of the cerebellum: hypothesis for function.," J Integr Neurosci, vol. 10, pp. 317-352, 2011.

[31] N. R. Luque, J. A. Garrido, R. R. Carrillo, S. Tolu, and E. Ros, "Adaptive cerebellar spiking model embedded in the control loop: context switching and robustness against noise.," Int J Neural Syst, vol. 21, pp. 385-401, 2011.